Gas Mobility Patterns in Crystal Mush Analog Experiments

by
MaKayla Etheredge

A thesis accepted and approved in partial fulfillment of the

requirements for the degree of

Master of Science

in Earth Sciences

Thesis Committee:

Josef Dufek, Co-Chair

Katharine Cashman, Co-Chair

Paul Wallace, Member

University of Oregon

Summer 2024

THESIS ABSTRACT

MaKayla Etheredge

Master of Science in Earth Sciences

Title: Gas Mobility Patterns in Crystal Mush Analog Experiments

Volatile movement through crystal mush, which controls the efficiency of gas escape, is poorly understood. Previous studies using 2-D (Hele-Shaw) analog experiments show that the geometry (finger, fracture) and efficiency of gas escape is controlled by particle concentration. I extend this approach by adding photoelastic particles to track formation and destruction of force chains. 2-D analog (Hele-Shaw) experiments using solid particles (photoelastic disks), fluid (corn syrup), and gas (nitrogen) are used to quantify the role of varying injected gas flux (1000 cm^3/s to 10000 cm^3/s) on crystal and melt migration patterns. Experiments can be classified by gas geometry into fingering, transition and fracture regime; recorded pressure and light intensity provide a proxy for particle stresses caused by the gas flux rate.

ACKNOWLEDGEMENTS

Gratitude extends to all beings that have led to the success of this work. Thanks to Josef Dufek, Kathy Cashman, and Paul Wallace for their continuous optimism and guidance in the completion of this project. It was a honor to be a part of the wonderful lab group of Joe Dufek where every member welcomed me with open arms. Special thanks to closest people in the group who contributed unmeasurable support throughout the journey. Thanks to the members of my family who stand before and behind me, especially my mother, who provided a consistent reminder of encouragement and inner strength.

Last but not least, it is a privilege to have experience the land of what is now called Oregon. It was in the depths of nature where I have found my biggest source of truth and temperance. My sincerest gratitude and humbleness exude to these exchanges.

DEDICATION

Before I enter the rooms of your solitude
In my living form, trailing my shadow,

I shall have come unseen. Upstairs and down with you
And out across the roads and rocks to the river

to drink the cold spray. You will believe
a bird flew by the window, a wandering bee
buzzed in the hallway, a wind
rippled the bronze grasses. Or will you

know who it is?

Denise Levertov
“The Presence”

TABLE OF CONTENTS

LIST OF FIGURES

LIST OF TABLES

Tables

I. INTRODUCTION

Geologic Background and Motivation

Volcanic eruptions are driven by the exsolution and outgassing of gas in magma. Therefore, gas escape through magma is an indicator of eruption style [Cashman and Sparks, 2013]. Despite this understanding, there is still an uncertainty in small scale mechanisms of gas escape during volcanic eruptions [Christopher et al., 2015; Edmonds et al., 2022; Degruyter et al., 2019; Roche and Carazzo 2019]. Magma reservoirs are composed of three mechanical phases: crystal, melt, and gas. When considering only two phases of melt and gas in magma reservoirs, there is a scientific understanding of how viscosity plays a role in gas escape [Roche and Carazzo, 2019; Saffman and Taylor, 1958]. High viscosity melt can cause gas to migrate more slowly due to the fluid resisting gas movement, making it harder for the gas to overcome drag forces that oppose mobility. Low viscosity melt can allow gas to escape more quickly due to the fluid offering less resistance to gas movement. However, the addition of crystals complicates understanding of gas-magma-crystal interactions. Additionally, these interactions will change as magmas crystallize at different rates and produce different concentration of crystals [Bergantz et al., 2017; Dufek and Bachmann, 2010].

Outgassing in crystal-poor magma occurs via a relatively short mean free path of gas in the melt [**Figure 1a]**. In magma with high crystal contents (>50%; crystal mush), gas mobility is influenced by the more tortuous path [**Figure 1b]**. Detailed knowledge of these forms and pathways of gas in crystal mush magma composition is limited [Degruyter et al., 2019]. Understanding gas escape patterns in crystal mush zones is important not only because they dominate many magmatic systems, but they often lead to explosive volcanic eruptions [Christopher et al., 2015; Edmonds et al., 2022; Suckale et al., 2016]. Understanding this complicated small scale three phase behavior in a crystal mush zone is therefore important for understanding volcanic processes and predicting volcanic eruption hazards.

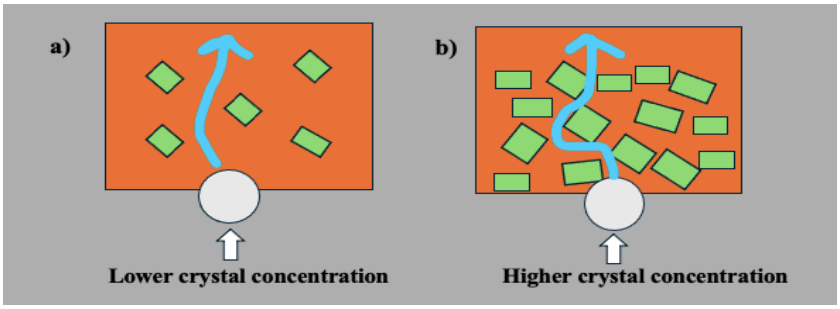

Figure 1: a) Schematic of magma reservoir with lower crystal concentration. Due to low crystal content, gas (white circle) can freely move in melt (orange box) and around crystals (green squares). **b)** Schematic of magma reservoir with higher crystal concentration. Due to high crystal content gas (white circle) cannot easily move in melt (orange box) and around crystals (green squares), creating uncertainty in small scale processes.

Previous studies have approached this problem with analytical investigations and numerical models [Burgisser and Bergantz, 2011; Higdon, 2013; Parmigiani et al., 2014]. Limits to analytical investigations include the computational and numerical difficulty of mimicking natural conditions. An emerging approach to this problem is to use analog experiments in laboratory settings to analyze the primary dynamics of a simplified system. These experiments are valuable when direct observation of natural phenomena can be challenging or impossible. Analog experiments can provide a tactile and controlled environment to explore questions about small (cm) scale volatile degassing in magma reservoirs. Previous studies have begun to answer aspects of these questions; however, the foundation of these answers is still being constructed. This study aims to build on the foundation of this emerging research.

Experimental Background

Observations of experiments analogous to magma reservoirs have successfully recorded small-scale gas mobility patterns through particle rich suspensions [Belien et al., 2015; Meng et al., 2022; Oppenheimer et al., 2015;2020]. One previous investigation (Oppenheimer et al., 2015) observed the effect of varying particle concentration in magma on the geometric form of gas escape with the use of a Hele-Shaw cell **[Figure 2].** A Hele-Shaw cell is an experimental apparatus used to study the behavior of fluid flow in a thin gap between two parallel plates. A Hele-Shaw cell effectively provides a 2-D perspective. Oppenheimer et al. (2015) used a Hele-Shaw cell (dimensions 40 × 40 × 2 cm) and magma reservoir analog components to observe three phase experiments (particles (crystals), gas, and corn syrup (melt)).

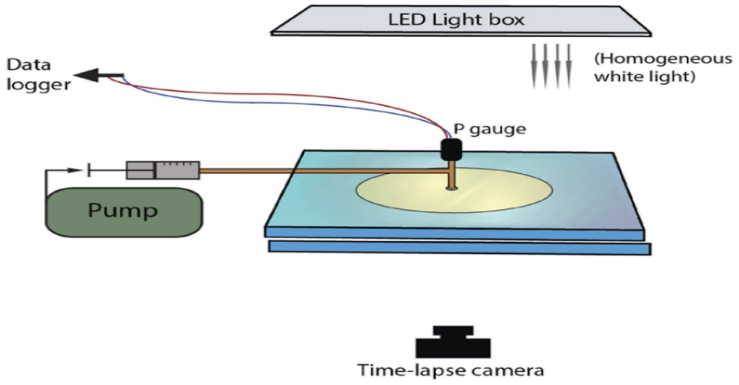

Figure 2: Hele-Shaw cell (dimensions 40 × 40 × 2 cm) setup from Oppenheimer et al. (2015)

When varying particle concentration (0-55%) and keeping a constant gas flux of 52 mL/h, Oppenheimer et al. (2015) observed three main geometric forms as modes of gas escape. The first form are finger instabilities, defined as a slow percolation of gas through the particle system in the form of gas 'fingers' **[Figure 3a]**. The second form is the fracture regime, defined as a fast and abrupt movement of gas through narrow fractures. An intermediate transition regime is defined by the presence of both fingers and fractures in the system.

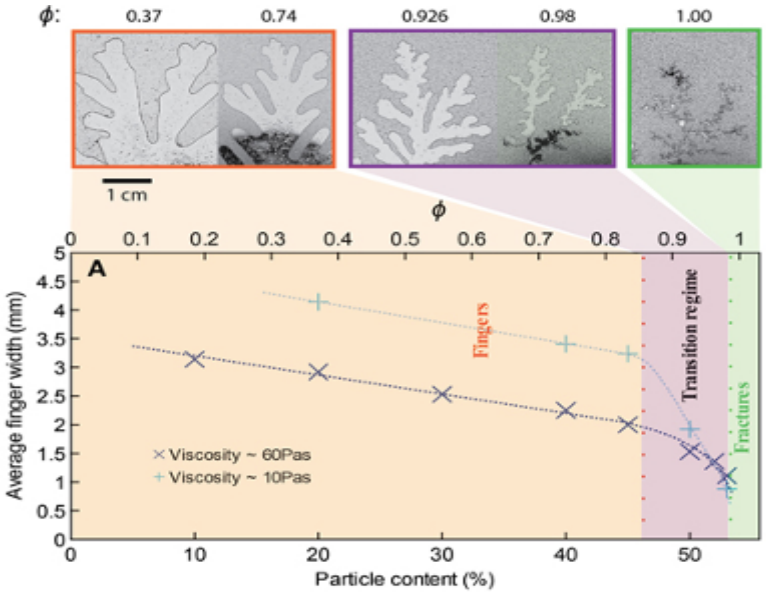

Figure 3: Edited Oppenheimer et al., 2015 graph showcasing results of 2-D (Hele-Shaw) analog experiments. During 0% to ~45% particle concentration, there is a recording of a fingering regime (orange box), between ~45% to 55% particle concentration, there is a transitionary

regime (purple box), and above ~55% particle concentration, there is a recording of a fracturing regime (green box) in the experimental system.

Particle concentrations of 0% to ~45% produced a fingering regime; between ~45% to 55% particle concentration produced a transitionary regime, and > ~55% particle concentration produced a fracturing regime in the particle suspension [**Figure 3**]. Qualitatively, with every other variable constant in the system, these experiments would suggest that a low crystallinity magma reservoir would permit gas escape in the form of fingers. Inversely, a high crystallinity magma reservoir with magma would be more prone to a fracture mode of gas escape.

Meng et al. (2022) used a 2-D Hele-Shaw cell (10.6 cm radius) to observe particle behavior in granular suspensions **[Figure 4]**. These experiments can be applicable to many disciplines including magma reservoir dynamics. In their investigations, they used a fixed gas flux (100 ml/min) and a limited range in particle concentration (78 and 84%), and observed fluid induced deformation on particle behavior. The analog components used consisted of silicon oil (melt)), gas, and photoelastic particles (crystals). Observation of fluid induced deformation on particle behavior or forces enacted on crystals is an important process in degassing. In a magma reservoir, crystals have the potential to jam and accumulate large amounts of force [Oppenheimer et al., 2015; Parmigiani et al., 2016]. This can cause a pressure increase leading to a destabilization of the magma reservoir and potential eruption [Bergantz et al., 2017]. Understanding the overall stresses on crystals in experiments improve understanding of degassing and gas and melt properties that lead to an eruption.

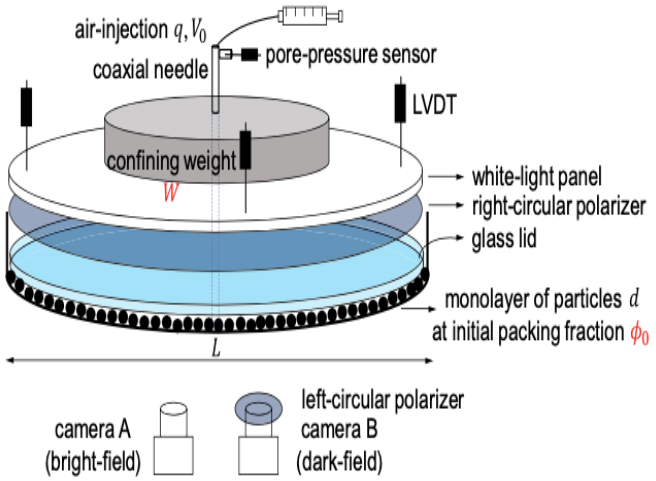

Figure 4: Meng et al. (2022) Hele Shaw cell (10.6 cm radius) setup.

The analog component of photoelastic particles allows analysis of forces on individual particles. Photoelastic particles have been used previously in a variety of experiments in granular physics and engineering [Estep and Dufek, 2013; Li et al., 2015]. When stressed under circularly or plane-polarized light, the photoelastic disks become birefringent due to deformation **[Figure 5a]**. This birefringent pattern often appears in the form of force chains, linear features that transmit forces in granular materials [Daniels et al., 2017] **[Figure 5b]**. For small stresses, the intensity of propagated light in photoelastic disks is approximately linearly related to the applied stress, enabling a convenient way to measure stresses on distributed particles [Abed Zadeh et al., 2019]. For particles with material properties similar to the urethane particles used in these experiments (and the experiments presented below), the linear relationship should be valid for forces less than approximately 0.2 N, although further work should be performed to confirm this. This approach thus provides a visual way to qualitatively and quantitatively record the intensity of force in the system during experiments.

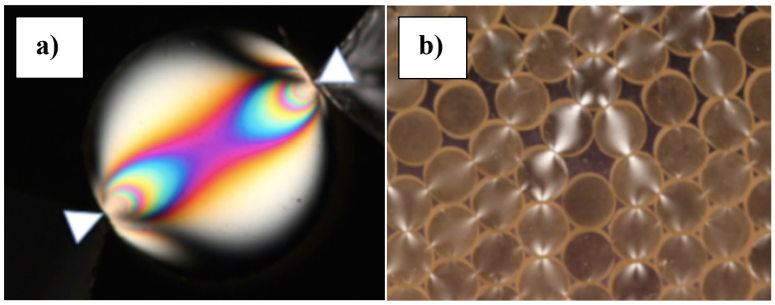

Figure 5: a) Stress pattern observed on a single photoelastic disc within a force chain, the white triangles indicate the points of applied force [Estep and Dufek, 2013]. **b)** Stressed photoelastic force chains [Estep and Dufek, 2013].

In their experiments, Meng et al. (2022) found that particles in the finger regime recorded less force intensity than in the fracture regime **[Figure 6]**. This can provide some understanding into the threshold phenomena for fracture conditions in a magma mush regime with implications for eruption initiation.

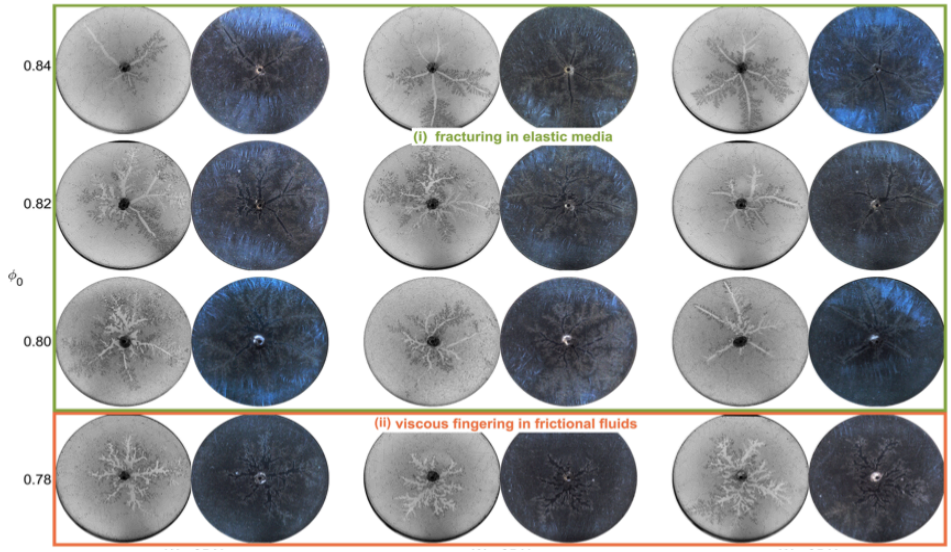

Figure 6: Meng et al., 2022 diagram showcasing results of 2-D (Hele-Shaw) analog experiments. During finger particle concentration regime, there is a lower photoelastic intensity and in the fracture regime particle concentration regime, there is a higher photoelastic intensity in the experimental system.

Oppenheimer et al. (2015) and Meng et al. (2022) provided insight into the origin of some gas mobility behavior patterns in magma reservoirs but left questions unanswered. One unanswered question is the effect of gas flux on high particle concentration magma because it is likely that crystal mush zones experience variable rates of gas flux [Bergantz et al., 2017; Burgisser and Bergantz 2011]. This study aims to further explore gas mobility migration by investigating the finger, transition, and fracture regime shift in relationship to gas flux rate instead of particle concentration. This study also aims to investigate the effect of gas flux variance on the system with using photoelastic particles as a crystal analog to study forces on the solid matrix. Lastly, this study aims to improve the previous studies by recording gas pressure in the analog system to quantify the pressure variance activity through the system. Overall, these simple analog experiments aim to strengthen small scale understanding of crystal mush systems, with associated implications for magmatic systems.

The objective of this study is to analyze three gas, crystal, and melt behavior in 2-D Hele-Shaw analogue experiments by varying gas flux rate:

1. **Behavioral finger, transition, fracture regime shift**

2. **Behavioral pressure activity in end members experiments**
3. **Force intensity variance in end member experiments**

II. METHODS

Experimental Setup

The Hele-Shaw apparatus is a specialized experimental setup used to study the behavior of fluid flow in a thin gap between two parallel plates **[Figure 7b]**. To observe gas mobility, analog experiments were conducted using solid particles (photoelastic disks, 6mm), gas (nitrogen), and fluid (corn syrup, 50-100 Pas). The Hele-Shaw cell consists of two (40 x 40 cm dimensions) glass plates with a horizontal void space (10.16 cm diameter) in the center **[Figure 7b]**. In the midpoint of the upper plate, there is an insert (2.54 cm diameter) which allows for the connection of two plastic pipes **[Figure 7c]**. A plastic pipe (2.54 cm diameter) is connected to a mass flow controller (MKS 1179C) to record flow rate (cm^3/min) and another smaller plastic pipe (1.27 cm) is connected to a pressure transducer (MPX5010DP Board Mount Pressure Sensor) to record the pressure difference between atmospheric pressure (kPa) and the pressure in the system (kPa). The controller and pressure transducer are monitored through an Arduino code and board **[Appendix 2]**.

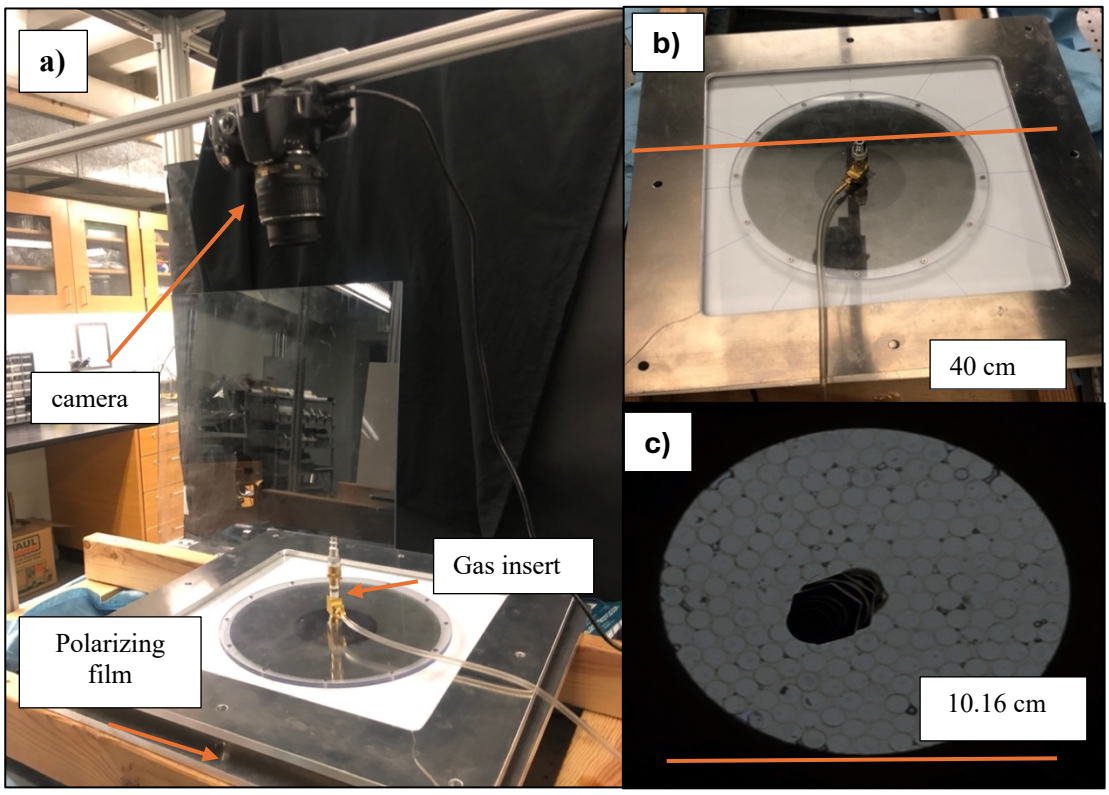

Figure 7: a) Full experiment setup with Hele-Shaw cell and camera propped above. Gas insert is labelled **b)** Above view of Hele-Shaw cell **c)** Beginning setup of void space.

A uniform light source emits light to the system from below. A LED light attached to the system lights up when the experiment starts, queued by an Arduino code to synchronize measurements. One circular polarizing film placed above the upper glass plate and one circular polarizing film is placed below the bottom glass plate to create cross polarization. Finally, a Nikon 3400 camera is suspended above to record experiments.

Before an experiment is conducted, photoelastic disks are placed face down into the void space in the Hele-Shaw cell at random close packing until the space is filled. Corn syrup is then seeped down into the void space until every disk is covered and the void space is filled with corn syrup **[Figure 7c]**. The volume fraction of particle and corn syrup is ~69% for each experiment. After the corn syrup is drained, the other glass plate is placed on top of the void space, then the polarizing sheet. The plastic pipe that will carry nitrogen gas is inserted. The camera is then turned on to record. A gas flux rate (cm^3/min) is specified in the Arduino code **[Appendix 2]**, and is triggered to start with a thirty second delay. A python code in Spyder IDE is simultaneously triggered to record pressure (kPa) in the system **[Appendix 3]** via the pressure transistor at the entrance of the gas to the Hele-Shaw cell. The experiment begins at the initiation of the gas flux.

Experimental Procedure

To study gas patterns in the three phase analog experiments, several experiments were conducted in one thousand cm^3/min increments from 1000 to 10000 cm^3/min to first categorize the fingering, transition, fracturing regime.

Gas Flux Rate (cm^3/min) Total Nr of experiments: 25	**Observed Regime (Finger, Transition, Fracture)**
1000 cm^3/min (4) , 2000 cm^3/min (3), 3000 cm^3/min (3) , 4000 cm^3/min (2), 5000 cm^3/min (2), 6000 cm^3/min (3), 7000 cm^3/min (2), 8000 cm^3/min (1), 9000 cm^3/min (1), 10000 cm^3/min (4)	?

Table 1: Experiment table showcasing total number of experiments ran at each gas flux rate to observe geometric regimes.

Pressure transducers record gas pressure evolution throughout the duration of the experiment. Post processing of the end member data (1000 and 10000 cm^3/min) to observe variance in light intensity included creation of a MATLAB script that reads each frame of the video then converts it to grayscale **[Appendix 1]**. To assess variations in light intensity, the grayscale image is then normalized so that the minimum pixel value is 0 and the maximum pixel value is 1, then standard deviation of the normalized pixel intensities is calculated. This normalization ensures that the background is set to black (0) before calculating the contrast value. Finally, the script will plot the intensity values over the length scale of the video.

Gas Flux Rate (cm^3/min) Nr of experiments: 6	Pressure and Crystal Force Intensity Variance (kPa)
1000 cm^3/min (3)	?
10000 cm^3/min (3)	?

Table 2: Experiment table showcasing total number of experiments ran at each gas flux rate to observe pressure and crystal force intensity variance.

III. RESULTS

Geometry Regime

Experiments conducted at gas flux rates of 1000, 2000, 3000, 4000, 5000, 6000, 7000, 8000, 9000, and 10000 cm^3/min recorded a series of gas escape regimes. The finger regime is defined as a slow percolation of gas through the particle system, the fracture regime is defined as a fast and abrupt movement of gas through the particle system, and the transition regime includes both fingers and fractures. Using these definitions, experiments conducted at 1000 cm^3/min recorded a finger regime. Experiments at 2000, 3000, 4000, 5000 cm^3/min recording a transition regime. Experiments at 6000, 7000, 8000, 9000, 10000 record a fracture regime.

Finger Regime

The following images show the finger regime recorded at 1000 cm^3/min gas flux. During all experiments, gas pockets (fingers) slowly maneuvered through the pore space between particles starting at the gas injection midpoint and continuing to the edge of the suspension. In contrast to the low flux experiments of Oppenheimer et al. (2015), in this regime the particles had minimal displacement. Example of fingers captured in experiments are shown in **Figures 8.1c and 8.2c** (see the gray gas pockets in red boxes). The average velocity of gas throughout experiments was ~ 0.18 cm/s. Qualitatively, overall force or light intensity on particles in the system moderate with limited force chain development, including near the fingers.

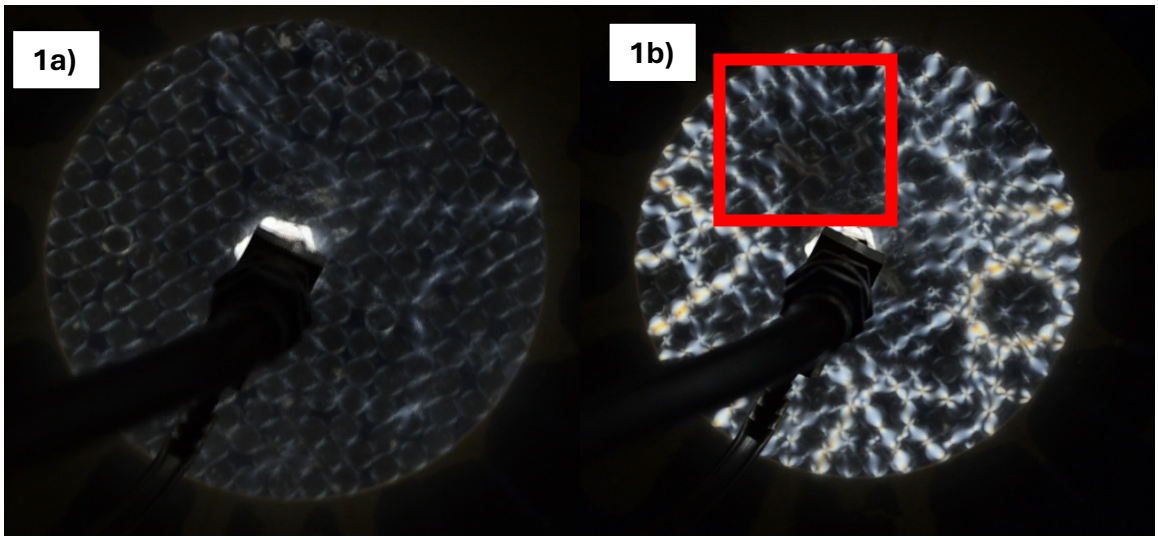

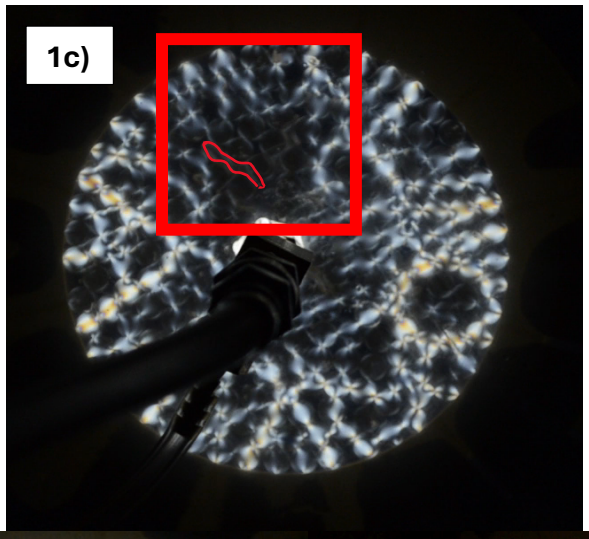
1c)

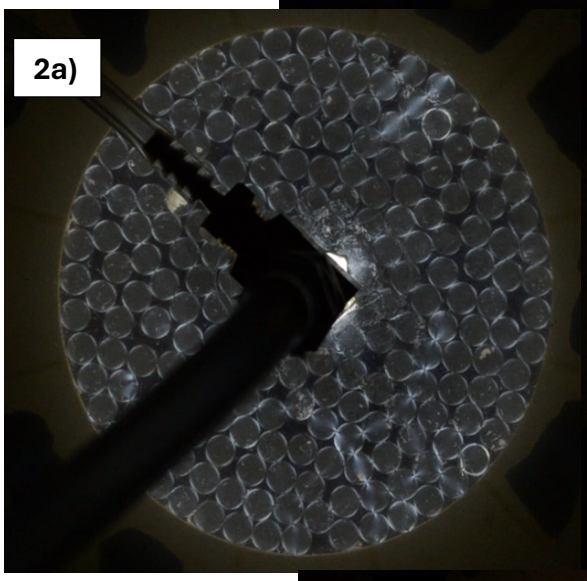
2a)

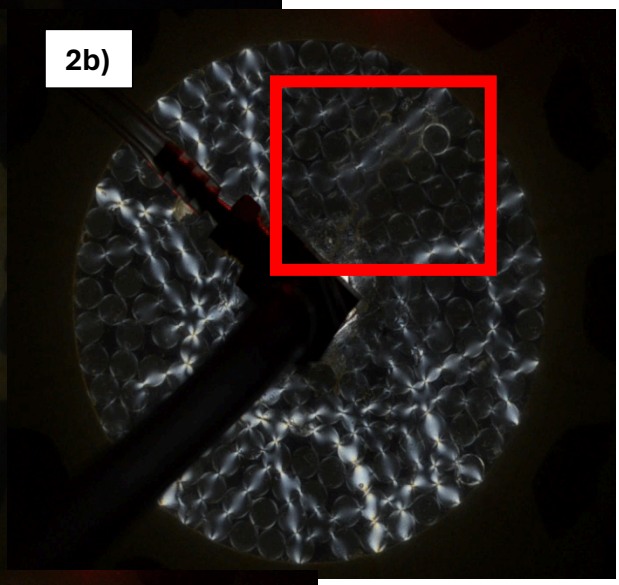
2b)

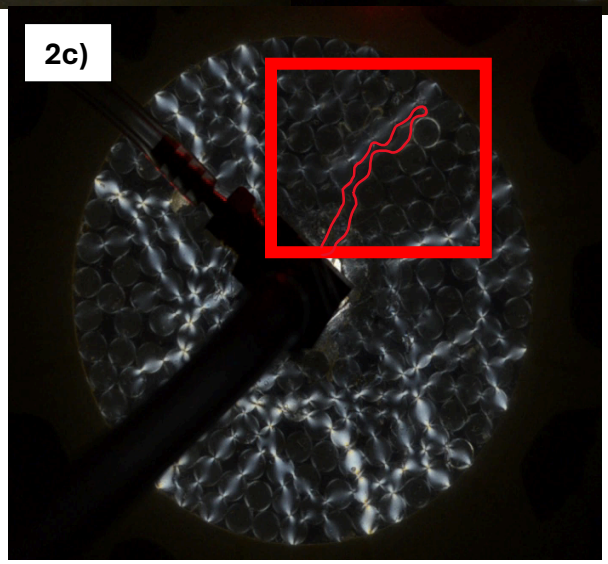
2c)

Figure 8: Recorded finger regime at 1000 cm^3/min gas flux rate. **1a)** Before experiment one is conducted at 1000 cm^3/min gas flux rate. **1b)** During experiment one at 1000 cm^3/min gas flux rate with fingers highlighted in red box. **1c)** During experiment one at **1000** cm^3/min gas flux rate with finger outlined in red box **2a)** Before experiment two is conducted at 1000 cm^3/min gas flux rate. **2b)** After experiment two at 1000 cm^3/min gas flux rate with fingers highlighted in red box. **2c)** During experiment two at **1000** cm^3/min gas flux rate with finger outlined in red box

Transition Regime

Figure 9 illustrates the transition regime recorded at 2000 to 5000 cm^3/min gas flux. The transition regime is defined by the presence of both fingers and fractures in an experiment. During experiments, gas pockets (fingers) slowly moved throughout pore space between particles starting at the gas injection midpoint. Once the gas reached around halfway to the edge of the suspension, however, gas pockets quickly move to the edge of the suspension as fractures. Particles in these experiments had more displacement compared to the finger regime. Examples of fingers captured in experiments are gray gas pockets denoted in red boxes **[Figure 9.1a and 9.1b]**. Example of fractures routes captured in experiments are denoted in blue boxes **[Figure 9.1c and 9.1d]**. Fractures in these experiments occur abruptly, therefore capturing this gas pattern in this regime is difficult. However, the remnant fracture route is captured as the region where the disks are not stressed (highlighted in **Figure 9c)**. The average velocity of gas escape during transition experiments was ~ 0.87 cm/s.

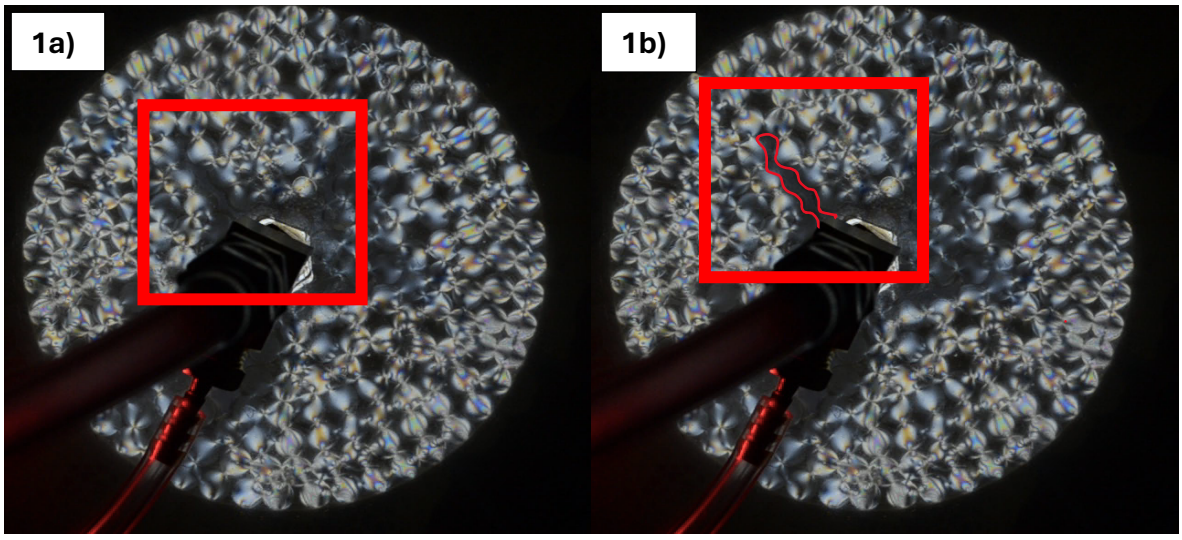

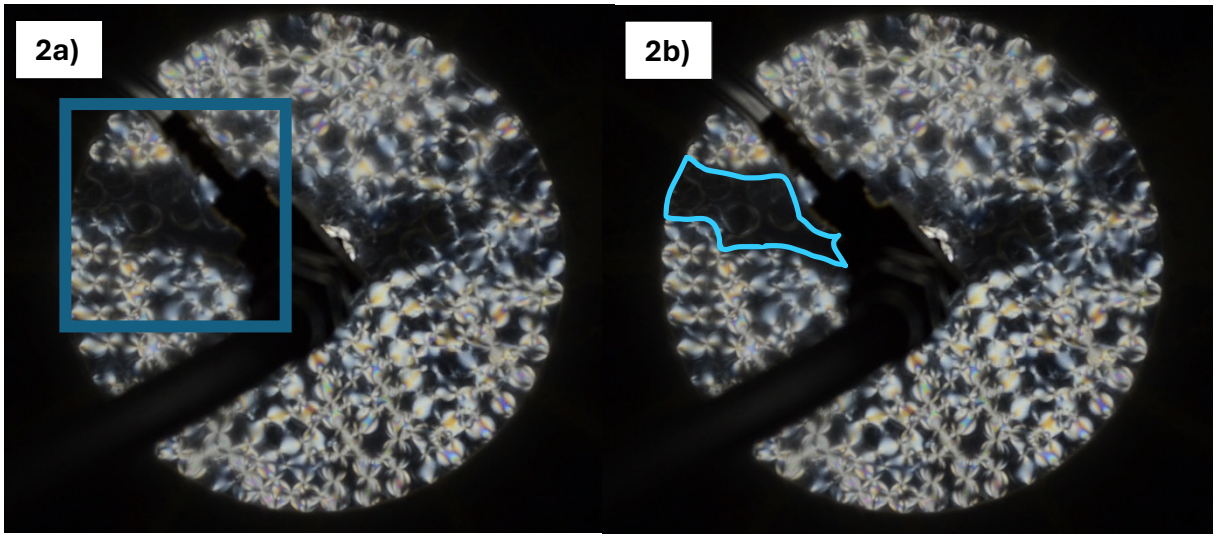

Figure 9: Examples of fingers and fractures recorded in the dominated transition regime of 2000 to 5000 cm^3/min gas flux rate. **1a)** 3000 cm^3/min gas flux experiment with finger in red box **1b)** 3000 cm^3/min gas flux experiment with finger in red box outlined **2a)** 2000 cm^3/min gas flux with finger in red box **1b)** During experiment 2000 cm^3/min gas flux with finger in red box outlined.

Fracture Regime

Figure 10 showcases the fracture regime recorded at 6000 to 10000 cm^3/min gas flux. During all experiments, gas pockets (fractures) quickly moved to the edge of the suspension. Many fractures that reached the edge of the suspension opened and then quickly resealed. The particles in these experiments had the most displacement of all regimes. Example of fractures captured in experiments are denoted in blue boxes **[Figure 10]**. The average velocity of fractures throughout experiments was ~ 2.2 cm/s. Qualitatively, the overall force (light intensity) on particles in the system was higher than in both finger and transition regimes, with every particle being part of a force chain shortly after the start of experiments. There was also a noted acoustic difference in this regime compared to other regimes. Experiments in the fracture regime produced loud sounds due to quick pressure build up and release.

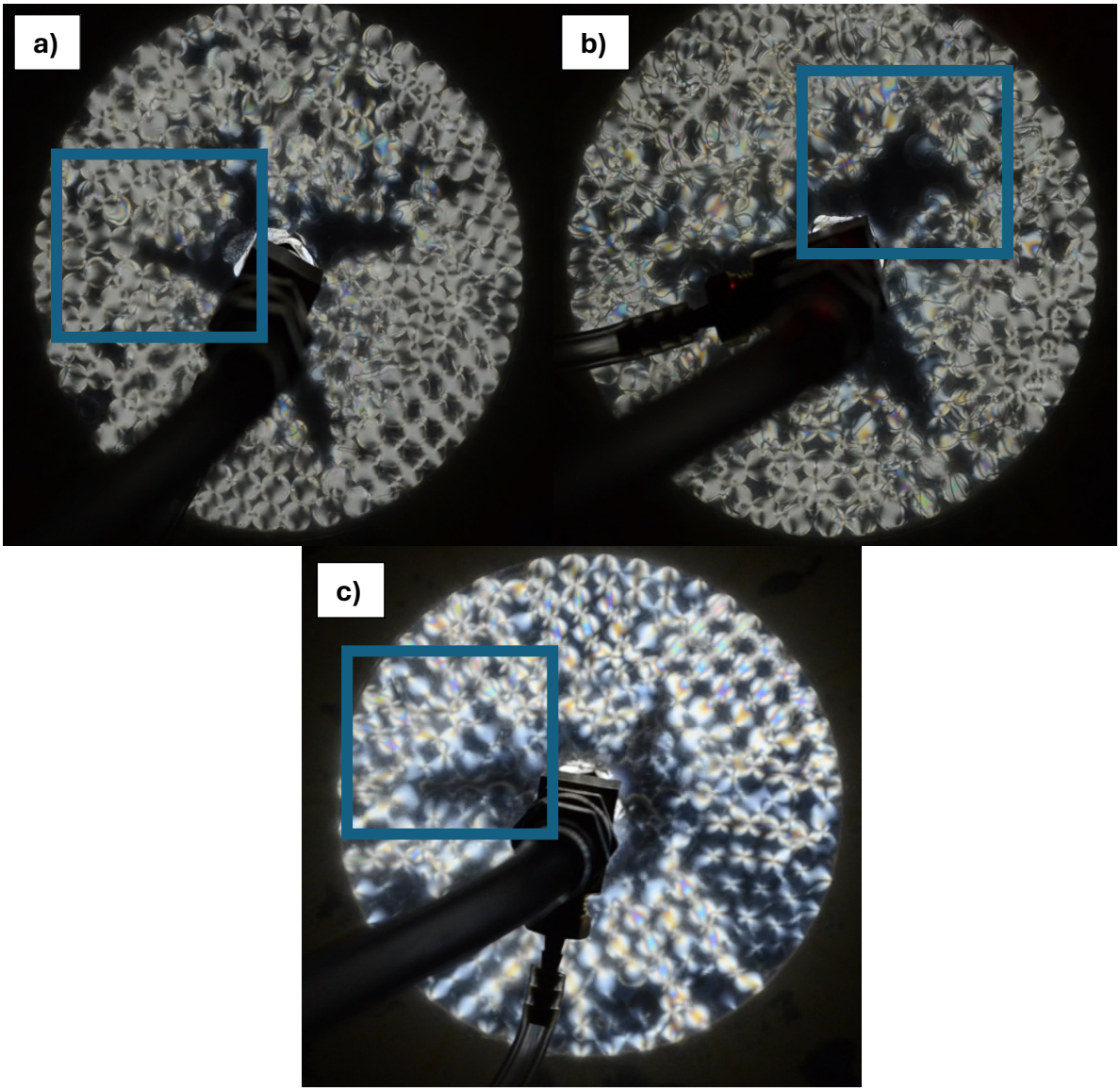

Figure 10: Examples of fractures (blue boxes) recorded in the dominated fracture regime of 6000 to 10000 cm^3/min gas flux rate. **a)** 6000 cm^3/min **b)** 8000 cm^3/min **c)** 10000 cm^3/min

Pressure Variance for End Members

Experiments were conducted at 1000 cm^3/min and 10000 cm^3/min gas flux rates to record pressure variance in the suspensions. Highest and lowest gas flux rate show differences in pressure timeseries. The 1000 cm^3/min gas flux experiments recorded a spike in pressure slowly reaching ~ 8 and ~10 kPa, then stabilization **[Figure 11]** around the highest consistent pressure for that experiment. The 10000 cm^3/min gas flux experiments consistently demonstrate a quick

spike in pressure to above 10 kPa then a stabilization **[Figure 12]** around 6-10 kPa depending on the experiment.

Figure 11: Graphs of 1000 cm^3/min gas flux pressure measurements. Red box denotes example of pressure stabilization.

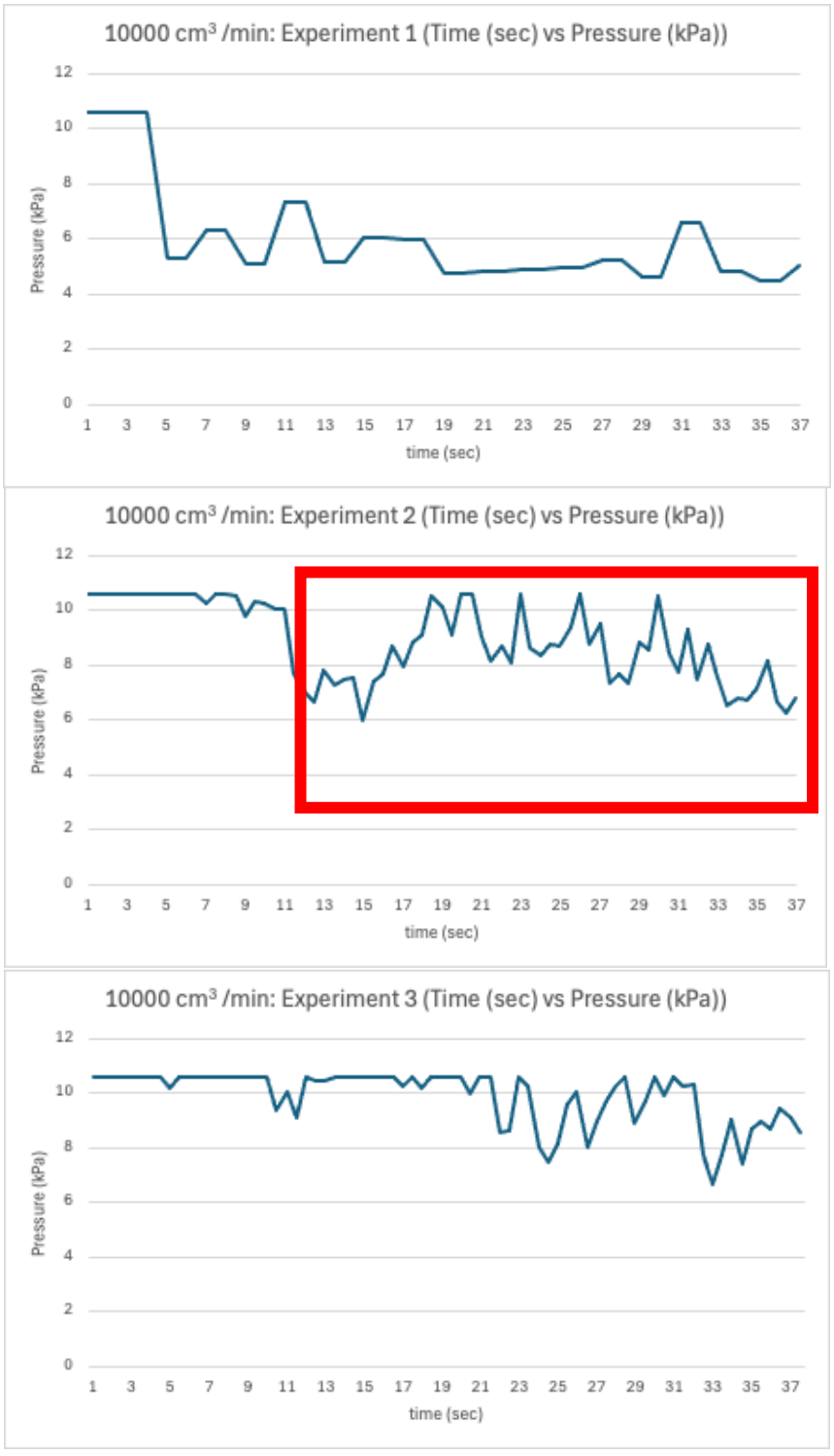

Figure 12: Graphs of 10000 cm^3/min time (sec) vs gas flux pressure measurements (kPa). Red box denotes example of pressure attempting to stabilize.

Light Intensity

Experiments conducted at 1000 cm^3/min and 10000 cm^3/min recorded light intensity variance. Light intensity was calculated using a MATLAB script **[Appendix 1].** The MATLAB script reads each frame and then calculates the standard deviation of the normalized pixel intensities. A value of 0 is the minimum value and a value of 1 is the maximum value. Comparatively, the 1000 cm^3/min end member recorded light intensity lower than the 10000 cm^3/min member. The 1000 cm^3/min experiments reached up to 0.15 light intensity value while 10000 cm^3/min experiments reached to almost 0.25. Experiment one of 1000 cm^3/min series recorded a gradual increase then decrease, then stabilization to around a consistent contrast value **[Figure 13]**. Experiment two and three of the 1000 cm^3/min series seem to gradually increase to stabilizition around a consistent contrast value. All the 10000 cm^3/min series of experiments recorded a quick increase to a high contrast value, then quick decrease to stabilization **[Figure 13]**.

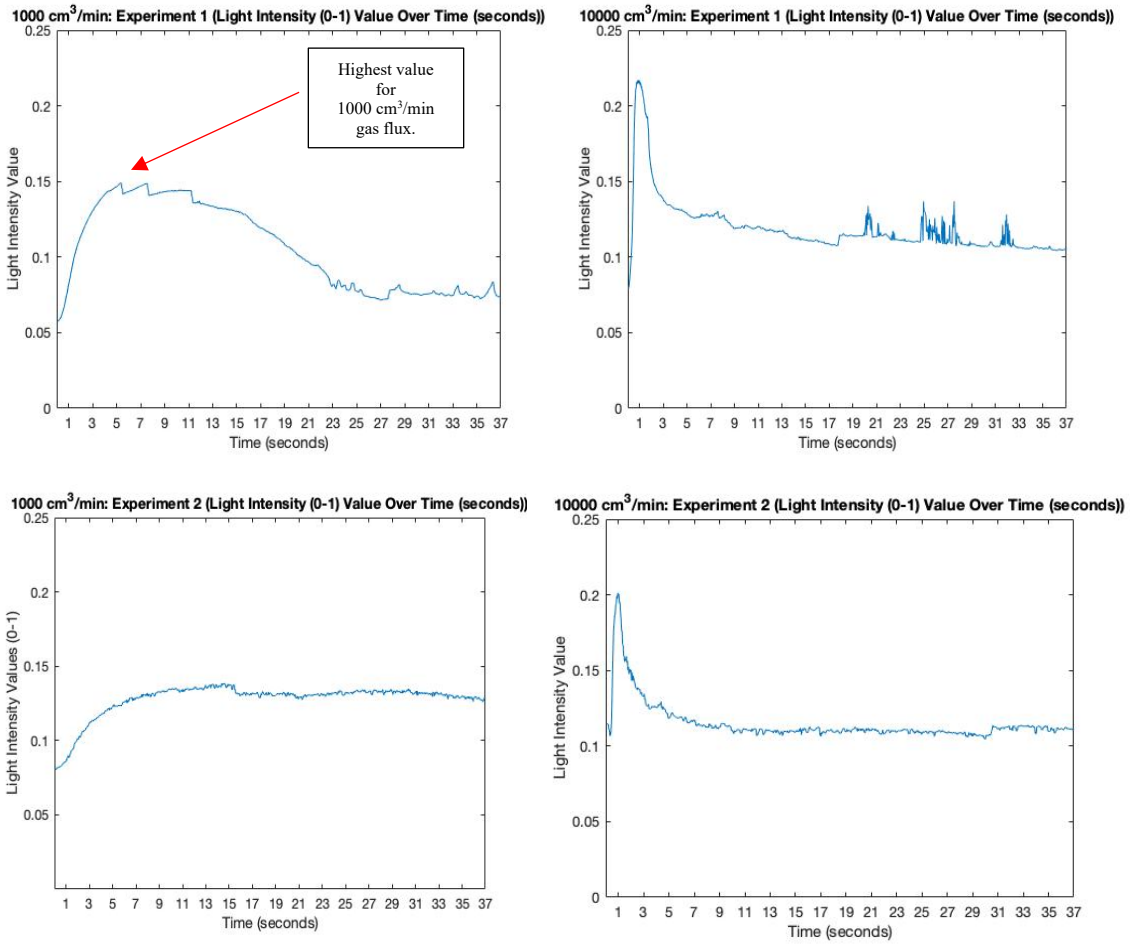

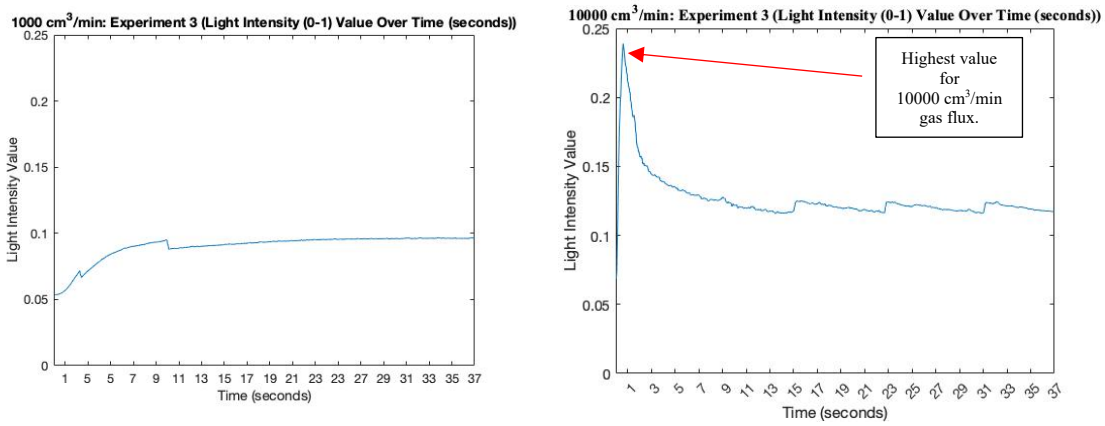

Figure 13: Graphs of all experiments at 1000 and 10000 cm^3/min gas flux light intensity value measurements (0-1) vs time (seconds). Red arrows denote differences in peak values between 1000 and 10000 cm^3/min gas flux light intensity values.

VI. DISCUSSION

Geometry Regime

Gas injection experiments conducted in a Hele-Shaw cell recorded three distinct regimes. At the 1000 cm^3/min gas flux rate, gas escaped in the form of geometric fingers **[Figure 8]**. The fingers moved around the particles in a random pattern slowly reaching the edge of the suspension. In contrast to Oppenheimer et al. (2015), where the fingering regime hosted wide gas fingers, in these experiments the fingers were small (< 4mm in width). Fingers were observed splitting around particles. Gas bubbles have been observed in a previous petrological study displaying similar patterns [Belien et al., 2010].

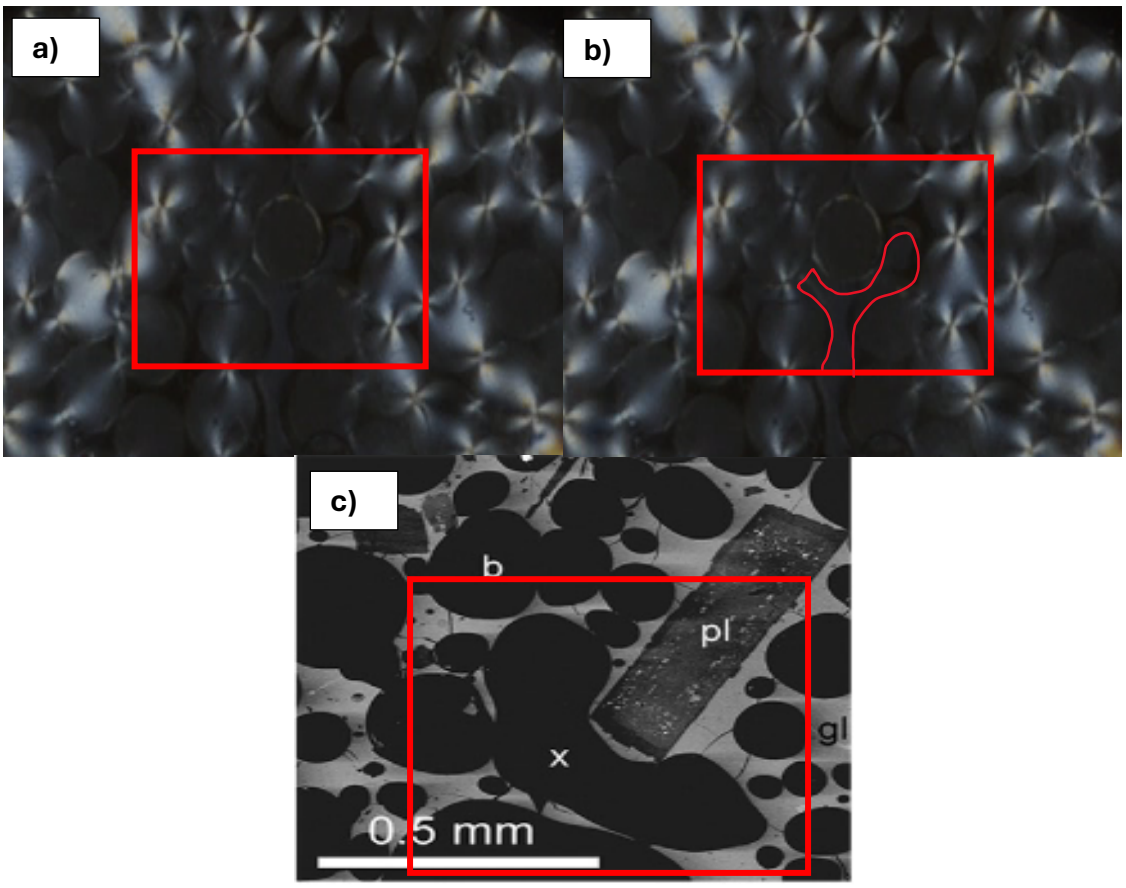

Figure 14: Comparison of splitting of gas in experimental studies vs observed petrological study. **a)** A 1000 cm^3/min finger (slow gas bubble) splitting around photoelastic particle (crystal) from Experiment 1 **b)** A 1000 cm^3/min finger (slow gas bubble) splitting around photoelastic particle (crystal) from Experiment 1, finger is traced in red **c)** Tephra from Stromboli Volcano showcasing a gas bubble splitting around plagioclase crystal [Belien et al., 2010]

At gas fluxes of 2000 to 5000 cm^3/min, gas moved from the injection midpoint and radially escaped in the form of both geometric fingers and fractures **[Figure 9]**. An experiment was denoted transitional if there was an observation of gas escape starting out as a slow percolation then abruptly escaping at the edge of the suspension. At gas flux rates of 6000 to 10000 cm^3/min, the gas moved from the injection midpoint and radially escaped out in the form of geometric fractures **[Figure 10]**. The fractures quickly displaced the particles as they reached the edge of the suspension.

Gas migration velocities varied with gas flux. For example, in observed videos, gas migration velocity during the 2000 cm^3/min experiments averaged ~0.84 cm/s **[Figure 16a]**, while at the 10000 cm^3/min the gas migration velocity averaged 2.54 cm/s **[Figure 16b]**. There was also a noted acoustic difference between the lower gas flux rates and higher gas flux rates, with the higher gas flux producing loud sounds due to quick pressure build up and release.

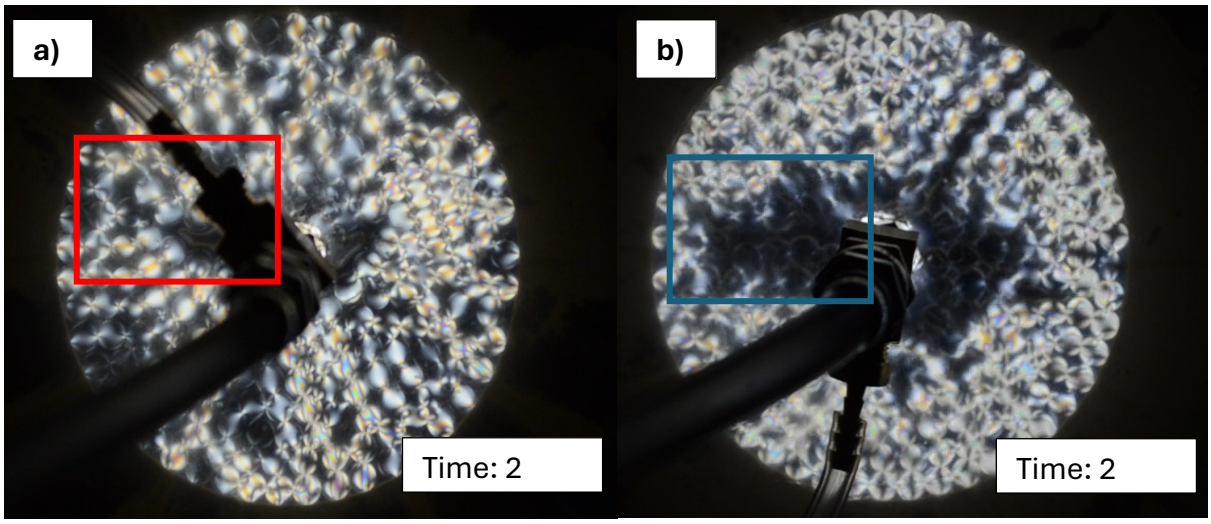

Figure 15: Comparison of **a)** 2000 cm^3/min (finger denoted in red box) vs **b)**10000 cm^3/min at 2 secs after the start of the experiment showcasing the higher gas flux rate contributing to quicker gas escape (remnant fracture route in blue box).

Pressure and Light Intensity Variance for End Members

Pressure was recorded for 1000 and 10000 cm^3/min end member gas fluxes. 1000 cm^3/min gas flux experiments recorded a slow spike in pressure then stabilization around the highest consistent pressure for that experiment **[**~10 kPa; **Figure 9]** while the 10000 cm^3/min gas flux experiments consistently demonstrate a quick spike in pressure then fluctuation between 8 and 10 kPa **[Figure 10]**. 1000 cm^3/min gas flux experiments could provide insight into a

continuous influx of gas forcing into a crystal mush that imposes a continuous stable pressure in the system. 10000 cm^3/min gas flux experiments could provide insight to a quick influx of gas forcing into a crystal mush that imposes an initial spike and inflation to the system, however soon after the gas has an efficient way to move out, the system deflates, and pressure attempts to stabilize. Fluctuations record opening and closing of fractures because of fluid (melt) migration into the open spaces.

Light intensity measurements showed that the light intensity (overall forces) increased with increasing gas flux. This result aligns with the observations of Meng et al. (2022), where the finger regime experiments recorded less brightness than the fracture regime experiments. Together these data can be used to understand threshold phenomena for fracture conditions in a magma mush regime, with possible implications for eruption initiation.

Visual evidence of force chains aligns with data on pressure and light intensity. For example, experiment two of the 1000 cm^3/min experiments shows a gradual increase of force chains expanding radially and then a decrease to stabiliz brightness. At the same time, the pressure increases gradually then stabilizes, and light intensity gradually increases then stabilizes **[Figure 17]**. All 10000 cm^3/min experiments, in contrast, show a quick rapid increase in force chain development followed by a decrease **[Figure 18]**. After initial release of gas escape, pressure is variable, while the light intensity stabilizes. Small episodic increases in light intensity, however, may correspond to observed pressure variations.

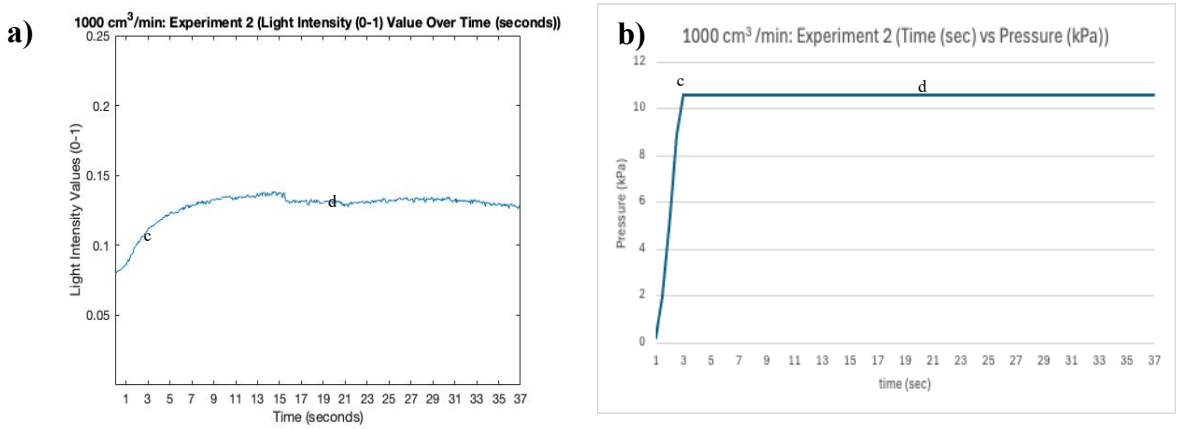

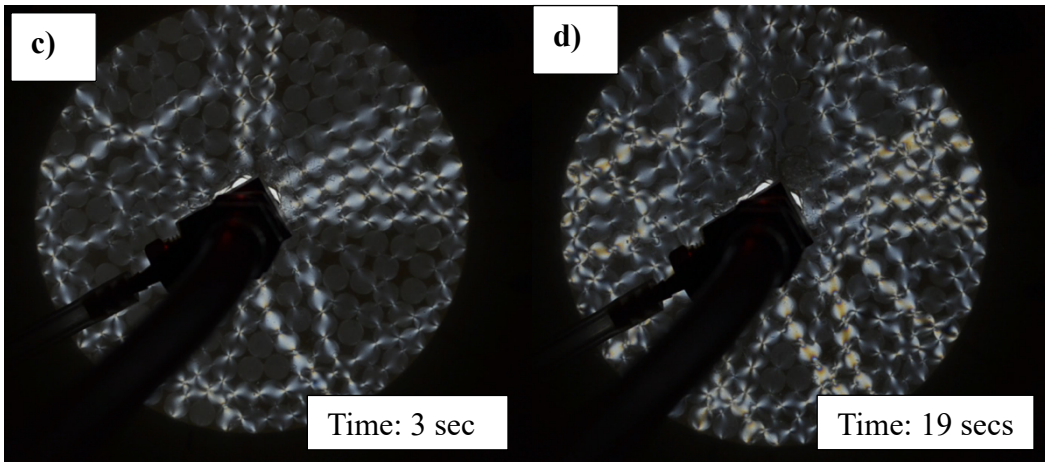

Figure 17: Comparison of 1000 cm^3/min **a)** light intensity values with letters c and d denoting correlating timestamp images and **b)** pressure graphs show alignment of general pattern of a quick increase starting at one second and one frame number then quick decrease (letters c and d denoting correlating timestamp images). **c)** Time stamp image of 1000 cm^3/min gas flux pattern at 3 secs **d)** Time stamp image of 1000 cm^3/min gas flux pattern at 19 secs.

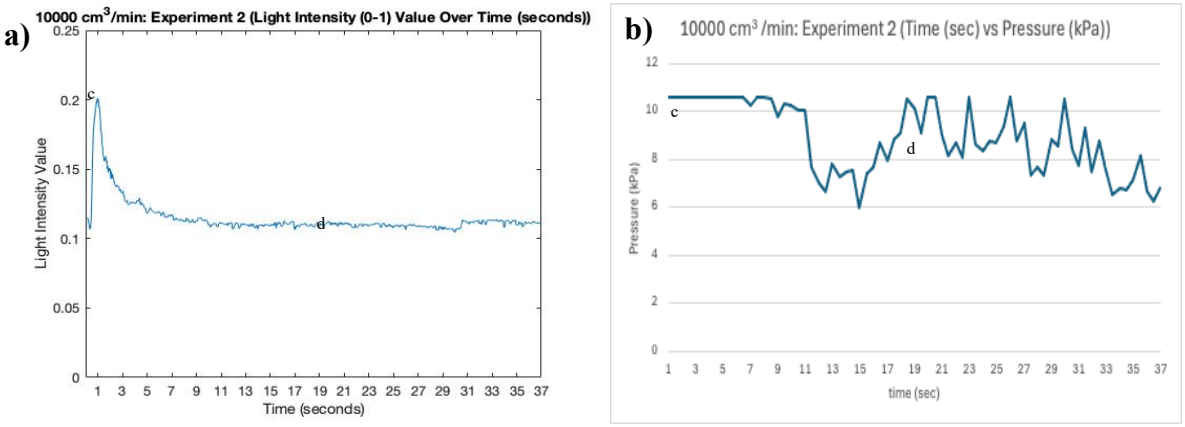

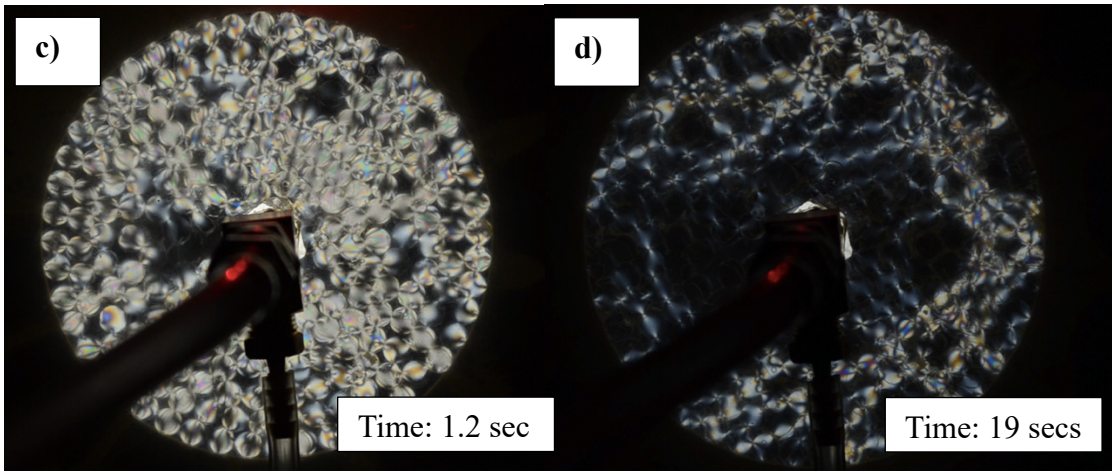

Figure 18: Comparison of 10000 cm^3/min **a)** light intensity values with letters c and d denoting correlating timestamp images and **b)** pressure graphs show alignment of general pattern of a quick increase starting at one second and one frame number then quick decrease (letters c and d denoting correlating timestamp images). **c)** Time stamp image of 10000 cm^3/min gas flux pattern at 1.2 secs **d)** Time stamp image of 10000 cm^3/min gas flux pattern at 19 secs

General Application to Natural World

Analog experiments conducted in this study are comparable to basaltic magmas that have >50% crystal content [Cashman and Edmonds, 2019]. Previous studies investigating basaltic magma mushes find similar mechanisms observed in the experiments [Christopher et al., 2015; Edmonds et al., 2022; Suckale et al. 2016]. Open vent volcanoes produce explosive, gas-rich eruptions that are triggered by the rise of exsolved volatiles from deeper crystal mush storage regions [Edmonds et al., 2022; Suckale et al. 2016]. Degassing mechanisms include an exsolved volatile phase that outgasses continuously from the volcano sourced from a mix of deep (second boiling) and shallow (convective degassing) source [Cashman and Edmonds, 2019; Ruth et al., 2018]. The findings of the lower gas flux rate experiments can be an example of this continuous passive degassing and magma rise to the shallow storage in a volcanic system. With the 1000 cm^3/min gas flux rate, there is an experimental observation of the fingers mentioned in this paper. The experiments showcase the continuous gas movement throughout the crystals that is slowly escaping. These experiments can build on this study by demonstrating a pressure and crystal force measurement within the magma mush zone during this time. During passive degassing in the magma mush, the crystal forcing perhaps is low and the pressure measurement seems to be at a consistent stabilized pressure.

High fluxes of deep exsolved volatile gas escape during volcanic activity at open vent volcanoes rise to pockets of exsolved volatiles that may ascend rapidly to the surface [Bergantz et al., 2017; Christopher et al., 2015; Edmonds et al., 2022]. With the 10000 cm^3/min gas flux rate, there is an experimental observation of this mechanism. The fractures (pockets of quick gas movement) in these high gas flux experiments may provide an experimental validity to the mentioned mechanisms at the beginning of an eruption. These experiments can also build on this study by showcasing a quick increase of crystal force and pressure measurement in the magma reservoir right at the start of the eruption. The acoustics of the higher gas flux rate can also provide some insight into increased seismic activity during an eruption.

Future Work

This study was conducted as a simple case to be used as a steppingstone for future investigations. Future work of this study may include varying photoelastic particle size and shape to better represent natural variablity. Additionally, further work is needed on detailed quantification of the forces imposed on crystal analogs. Specifically, measuring forces on crystals in contact with fingers and fractures could provide more detail on gas behavior in magma reservoirs. This would also strengthen the accuracy of future models of magma reservoirs. Photo-elastic Grain Solver (PEGS) is a MATLAB application that uses the G2 method to calculate the individual force of crystal particles in an image [Daniels et al., 2017]. Preliminary steps have been taken to use the PEGS MATLAB application [Daniels et al., 2017]. However, with the current experimental set up of the Hele-Shaw cell, PEGS was unable to be used for this study. Optimal use of PEGS requires both detection of the particle outlines and photoelastic pattern, and the current camera setup is not ideal for this arrangement. A future alternate setup of experiments with a smaller void space and a second camera would probably make using PEGS efficient.

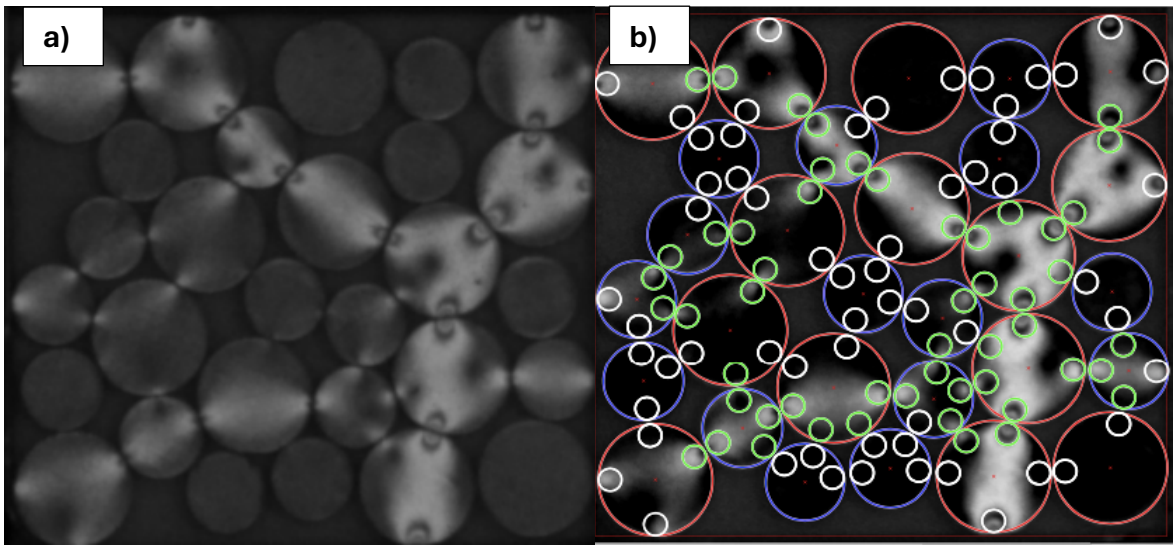

Figure 17: **a)** Daniels et al., 2017 sample image of forces on photoelastic disk used to be inputted int PEGS **b)** Daniels et al., 2017 sample output image of PEGS calculation of forces on photoelastic particle.

V. CONCLUSION

Small scale behavior in crystal mush is important in understanding viscous degassing. Simple 2-D (Hele-Shaw) analog experiments for crystal mush have successfully recorded small scale gas mobility patterns through particle rich suspensions. Experiments conducted with varying gas flux rate show a lower gas flux has an impact on gas mobility in the geometric form of fingers while a higher gas flux rate has an impact in the geometric form of fractures. Measurements of pressure in the suspension and forces enacted on crystals during end member experiments demonstrate other mechanisms that may be present in magma mush zones. Lower pressure and forces enacted on crystals were observed in lower gas flux rate and higher pressure and forces enacted on crystals were observed in higher gas flux rates. The findings in this study have applications to crystal mush studies conducted in the natural world. Lower gas flux experiments produced fingering instabilities with lower fluxes potentially similar to those observed during continuous degassing at open vent volcanoes. Higher gas flux experiments produced fracture deformation mechanisms similar to those observed during volcanic eruptions[Christopher et al., 2015; Edmonds et al., 2022; Suckale et al., 2016]. These fractures may be detectable with seismic arrays. Our findings contribute to improving the understanding and prediction of gas, crystal, and melt movement in crystal mush zones. This study demonstrates the value of experimental investigation and its opportunity to tactically explore small scale volcanic processes. Our study is an addition to the foundation of small-scale degassing understandings with simple experiments however more observations in the future are needed in this emerging research.

APPENDIX

```
% Define the path to the video file
videoFile = '10000may.mov'; % Update with your video file path
% Create a VideoReader object to read the video file
videoObj = VideoReader(videoFile);
% Get the number of frames in the video
numFrames = floor(videoObj.Duration * videoObj.FrameRate);
% Get the frame rate of the video
frameRate = videoObj.FrameRate;
% Initialize arrays to store contrast values and corresponding time for each frame
contrastValues = zeros(numFrames, 1);
timeInSeconds = zeros(numFrames, 1);

% Loop through each frame of the video
for frameIdx = 1:numFrames
    % Read the frame
    frame = readFrame(videoObj);

    % Convert the frame to grayscale if necessary
    if size(frame, 3) == 3
        grayFrame = rgb2gray(frame);
    else
        grayFrame = frame;
    end

    % Ensure the grayscale image is in double precision
    grayFrame = double(grayFrame);
    % Normalize the image so the minimum value is 0 (black background)
    minValue = min(grayFrame(:));
    maxValue = max(grayFrame(:));
    normalizedFrame = (grayFrame - minValue) / (maxValue - minValue);
    % Calculate the contrast value for the normalized frame
    contrastValues(frameIdx) = std2(normalizedFrame);
    % Calculate the time in seconds corresponding to this frame
    timeInSeconds(frameIdx) = frameIdx / frameRate;
end

% Plot the contrast values over time in seconds
figure;
plot(timeInSeconds, contrastValues);
xlabel('Time (seconds)','FontSize', 20);
ylabel('Light Intensity Value', 'FontSize', 20);
title('Light Intensity (0-1) Value Over Time (seconds)', 'FontSize', 20);
```

Appendix Figure 1: Example of Force Intensity Code

```
int setPoint = 3; // Or other PWM pin
int actual = A4;
//int input = 1000;
int number = 0;
//int CS1=10; //This example will use digital pin 10, as labeled on the arduino device. This will be for the LED
//that indicates the time before the flow controller starts.

int CS2 = 12; //This uses digital pin 11 to start a second LED that can be placed at the corner of the video frame that will
//start at the same time as flow controller starts.
//The long wire to the LED should be connected to the specified pins. The short needs to be connected to ground to
//complete the circuit.

const float ADC_mV = 4.8828125;       // convesion multiplier from Arduino ADC value to voltage in mV
const float SensorOffset = 200.0;     // in mV taken from datasheet
const float sensitivity = 4.413;      // in mV/mmH2O taken from datasheet
const float mmh2O_cmH2O = 10;         // divide by this figure to convert mmH2O to cmH2O
const float mmh2O_kpa = 0.00981;      // convesion multiplier from mmH2O to kPa
void setup() {
  pinMode(setPoint, OUTPUT);
  analogWrite(setPoint, 0);
  Serial.begin(9600);
  //delay(30000);
  //pinMode(CS2,OUTPUT);
}
void loop() {
digitalWrite(CS2,HIGH);
```

```
  // ((sensorValue in mV -sensorOffset)/sensitivity in mV/mmH2O)*kPa conversion constant
  float sensorValue = ((analogRead(A0) * ADC_mV - SensorOffset) / sensitivity *
mmh2O_kpa);     // result in kPa
  //float sensorValue = (analogRead(A0) * ADC_mV - SensorOffset) / sensitivity /
mmh2O_cmH2O;       // result in cmH2O

  Serial.print(micros());
  //delay(500);
  Serial.print(" , ");
 // Serial.println(sensorValue, 2);
  // using serial print format above, you can copy your data from the terminal,
  // paste it into NotePad app, than save as a .CSV file which can be opened in Excel
//void loop () {
  //if (Serial.available() > 0) {
    //Serial.readBytesUntil('\n', input, 1000);
    //number = atof(input)/1000*255;
    number = int(float(10000)/float(10000) *float(255));
    //Serial.println("Testing1:");
    //Serial.println(float(1000)/float(10000));
    //Serial.println("Testing 2");
    //Serial.println(int(float(1000)/float(10000)*float(255)));

    if (number < 0) number = 0;
    if (number > 255) number = 255; //8bit
    //TESTING
   // Serial.println(number);
    //take the next lines out...
   // Serial.print("Setting: ");
    //Serial.println(inputBuffer);
    // Serial.println(number);
   analogWrite(setPoint,number);
```

```
  //Serial.print("Actual flow rate: ");
  Serial.print(float(analogRead(actual))*(10000)/(1023)); //currently scaled to 11 bit data (0-
1023)
  Serial.print(",");
  Serial.println(sensorValue, 2);
   // Serial.println(",");
  delay(500);
}
```

Appendix Figure 2: Example of Arduino code

```
"""
import serial  #import serial library
import datetime
import time
import ast #import to parse string values between commas
from mpl_toolkits import mplot3d
import numpy as np
import matplotlib.pyplot as plt
# from drawnow import *
#-----------------------------------------------
#--2. Initialize some data files, etc
fig = plt.figure()
plt.ion()                       #For use of plotting figures in interactive mode
dataTimer =[]                       # empty list to store the data
dataFlow_Rate=[]
dataPressure=[]
#--3. Create a function for plotting interactively
def makeFig():
    plt.title('Example Photo Data')
    plt.grid(True)
    plt.xlabel('Time')
```

```
    plt.ylabel('Temp')
    plt.plot(dataTimer,dataFlow_Rate, color='red', marker='o',markerfacecolor='yellow')
    plt.savefig("dataout.png")

#ax = plt.axes(projection='3d')
x = datetime.datetime.now()
#--4. Set serial read information
arduino_port = "/dev/cu.usbmodem14201" #serial port of Arduino
baud = 9600 #match baud rate.
filename = "flow-pressure_data_seventhousand_julyeighth.csv" #name of the CSV file generated
ser = serial.Serial(arduino_port,baud)

#--5. Throwing away first string as before
time.sleep(.5)
b = ser.readline()         # read a byte string
#--6. Read and record the data

for i in range(140):
    b = ser.readline()         # read a byte string (to end of line)
    #print(b)
    string_n = b.decode()      # decode byte string into Unicode
    stringval = string_n.rstrip()  # remove \n and \r
    #First lets just log the value to a csv file
    file = open(filename, "a") #append the data to the file
    file.write(stringval + "\n") #write data with a newline
    #Next lets also convert it to data we can manipulate as floats
    #M=list(ast.literal_eval(stringval))
    #print(M[2])
    #Timer=float(M[0])          #convert time to float
    #Flow_Rate=float(M[1])   #convert flow rate to float
    #Pressure=float(M[2])    #convert flow rate to float
```

```
 # dataTimer.append(Timer)
  #dataFlow_Rate.append(Flow_Rate)
  #dataPressure.append(Pressure)
  #commented out 3D plot for now
#  plt.ion()
 # plt.plot(dataTimer,dataTemp, color='red', marker='o',markerfacecolor='yellow')
  #ax.scatter3D(dataTimer, dataTemp, dataPhoto, c=dataTemp, cmap='Reds');
  #drawnow(makeFig)
  time.sleep(0.5)
```

Appendix Figure 3: Example of Spyder IDE code

REFERENCES:

Abed Zadeh, A., Barés, J., Brzinski, T. A., Daniels, K. E., Dijksman, J., Docquier, N., Everitt, H. O., Kollmer, J. E., Lantsoght, O., Wang, D., Workamp, M., Zhao, Y., & Zheng, H. (2019). Enlightening force chains: A review of photoelasticimetry in granular matter. Granular Matter, 21(4). https://doi.org/10.1007/s10035-019-0942-2

Belien, I. B., Cashman, K. V., & Rempel, A. W. (2010). Gas accumulation in particle-rich suspensions and implications for bubble populations in crystal-rich magma. *Earth and Planetary Science Letters*, *297*(1–2), 133–140. https://doi.org/10.1016/j.epsl.2010.06.014

Bergantz, G. W., Schleicher, J. M., & Burgisser, A. (2017). On the kinematics and dynamics of crystal-rich systems. Journal of Geophysical Research: Solid Earth, 122(8), 6131–6159. https://doi.org/10.1002/2017jb014218

Burgisser, A., & Bergantz, G. W. (2011). A rapid mechanism to remobilize and homogenize highly crystalline magma bodies. *Nature*, *471*(7337), 212–215. https://doi.org/10.1038/nature09799

Cashman, K. V., & Sparks, R. S. (2013). How volcanoes work: A 25 Year perspective. *Geological Society of America Bulletin*, *125*(5–6), 664–690. https://doi.org/10.1130/b30720.1

Cashman, K., & Edmonds, M. (2019). Mafic glass compositions: A record of magma storage conditions, mixing and ascent. *Philosophical Transactions of the Royal Society A: Mathematical, Physical and Engineering Sciences*, *377*(2139), 20180004. https://doi.org/10.1098/rsta.2018.0004

Christopher, T., Blundy, J., Cashman, K., Cole, P., Edmonds, M., Smith, P., Sparks, R., & Stinton, A. (1970, January 1). *Crustal-scale degassing due to magma system destabilization and magma-gas decoupling at Soufrière Hills Volcano, Montserrat*. Apollo. https://www.repository.cam.ac.uk/handle/1810/248647

Daniels, K. E., Kollmer, J. E., & Puckett, J. G. (2017). Photoelastic force measurements in granular materials. *Review of Scientific Instruments*, *88*(5). https://doi.org/10.1063/1.4983049

Degruyter, W., Parmigiani, A., Huber, C., & Bachmann, O. (2019). How do volatiles escape their shallow magmatic hearth? *Philosophical Transactions of the Royal Society A: Mathematical, Physical and Engineering Sciences*, *377*(2139), 20180017. https://doi.org/10.1098/rsta.2018.0017

Dufek, J., & Bachmann, O. (2010). Quantum magmatism: Magmatic compositional gaps generated by melt-crystal dynamics. *Geology*, *38*(8), 687–690. https://doi.org/10.1130/g30831.1

Edmonds, M., Liu, E.J., Cashman, K.V., (2022) Open-vent volcanoes fuelled by depth-integrated magma degassing. *Bulletin of Volcanology*, 84:28 https://doi.org/10.1007/s00445-021-01522-8

Estep, J., & Dufek, J. (2013). Discrete element simulations of bed force anomalies due to force chains in dense granular flows. *Journal of Volcanology and Geothermal Research*, *254*, 108–117. https://doi.org/10.1016/j.jvolgeores.2012.12.023

Higdon, J. J. L. (2013, July 30). *Multiphase flow in porous media: Journal of Fluid Mechanics*. Cambridge Core. https://www.cambridge.org/core/journals/journal-of-fluid-mechanics/article/multiphase-flow-in-porous-media/A63CFE1696029299FD6867C29F57B0AB

Li, W., Meng, Y., Primkulov, B. K., & Juanes, R. (2021, August 25). Photoporomechanics: An experimental method to visualize the effective stress field in fluid-filled granular media. Physical Review Applied. https://www.osti.gov/pages/biblio/1852613-photoporomechanics-experimental-method-visualize-effective-stress-field-fluid-filled-granular-media

Meng, Y., Li, W., & Juanes, R. (2022, December 27). *Fracturing in wet granular media illuminated by photoporomechanics*. Physical Review Applied. https://journals.aps.org/prapplied/abstract/10.1103/PhysRevApplied.18.064081

Oppenheimer, J., Rust, A. C., Cashman, K. V., & Sandnes, B. (2015). Gas migration regimes and outgassing in particle-rich suspensions. Frontiers in Physics, 3. https://doi.org/10.3389/fphy.2015.00060

Oppenheimer, J., Capponi, A., Cashman, K. V., Lane, S. J., Rust, A. C., & James, M. R. (2020). Analogue experiments on the rise of large bubbles through a solids-rich suspension: A "weak plug" model for Strombolian eruptions. Earth and Planetary Science Letters, 531, 115931. https://doi.org/10.1016/j.epsl.2019.115931 Parmigiani, A., Faroughi, S., Huber, C., Bachmann, O., & Su, Y. (2016). Bubble accumulation and its role in the evolution of magma reservoirs in the Upper Crust. *Nature*, *532*(7600), 492–495. https://doi.org/10.1038/nature17401

Parmigiani, A., Huber, C., & Bachmann, O. (2014). Mush microphysics and the reactivation of crystal-rich Magma Reservoirs. *Journal of Geophysical Research: Solid Earth*, *119*(8), 6308–6322. https://doi.org/10.1002/2014jb011124

Roche, O., & Carazzo, G. (2019). The contribution of experimental volcanology to the study of the physics of eruptive processes, and related scaling issues: A Review. *Journal of Volcanology and Geothermal Research*, *384*, 103–150. https://doi.org/10.1016/j.jvolgeores.2019.07.011

Ruth, D. C., Costa, F., Bouvet de Maisonneuve, C., Franco, L., Cortés, J. A., & Calder, E. S. (2018). Crystal and melt inclusion timescales reveal the evolution of magma migration before eruption. *Nature Communications*, *9*(1). https://doi.org/10.1038/s41467-018-05086-8

Saffman PG, Taylor G. The penetration of a fluid into a porous medium or Hele-Shaw cell containing a more viscous liquid. Proc R Soc Lond Ser Math Phys Sci. (1958) 245:312–29. doi: 10.1098/rspa.1958.0085

Suckale, J., Keller, T., Cashman, K. V., & Persson, P. -O. (2016). Flow-to-fracture transition in a volcanic mush plug may govern normal eruptions at stromboli. *Geophysical Research Letters*, *43*(23). https://doi.org/10.1002/2016gl071501